JUNE 2017

CONFOCAL 3D RAMAN IMAGING

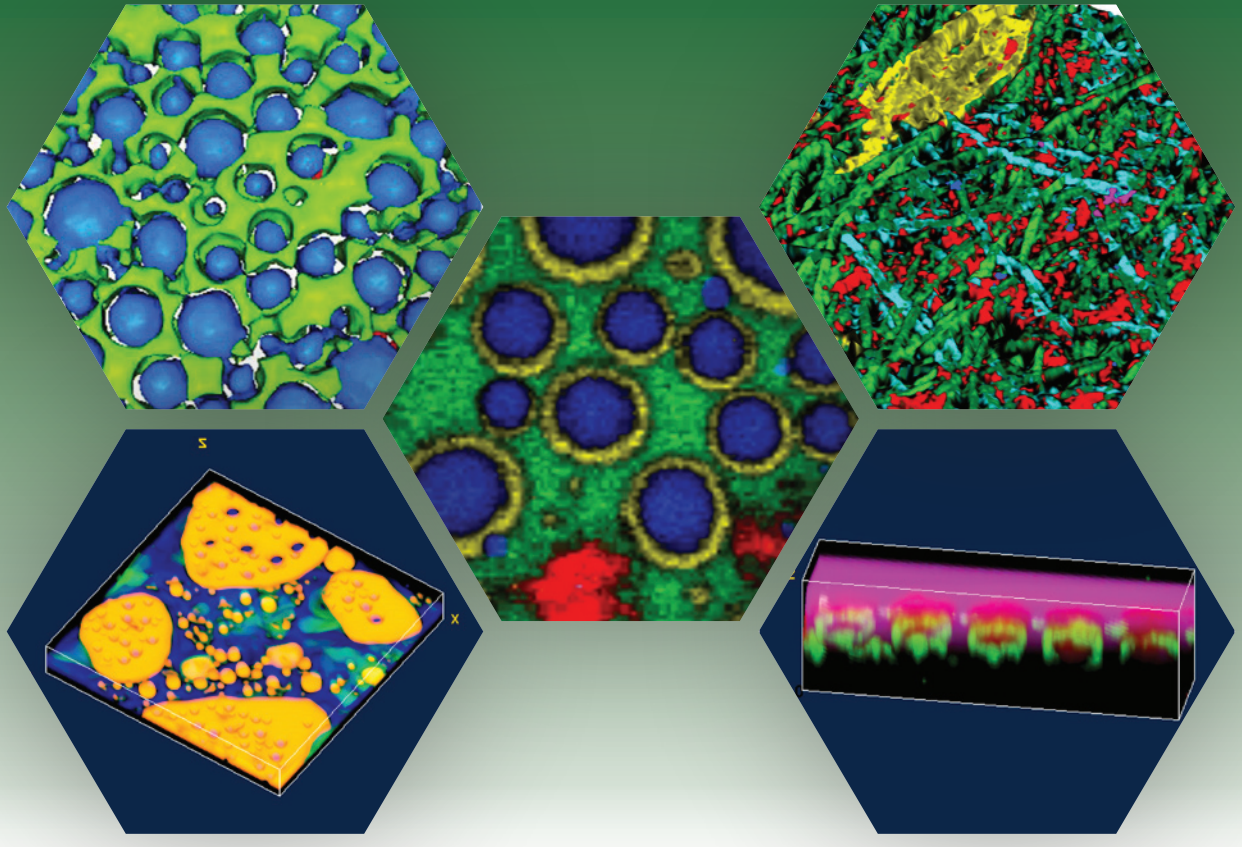

Sponsored by

WITec
focus innovations

Presented in partnership with

Spectroscopy

UBM

TOC
Table of contents

CONFOCAL 3D RAMAN IMAGING

Spectroscopy

UBM

WITec
focus innovations

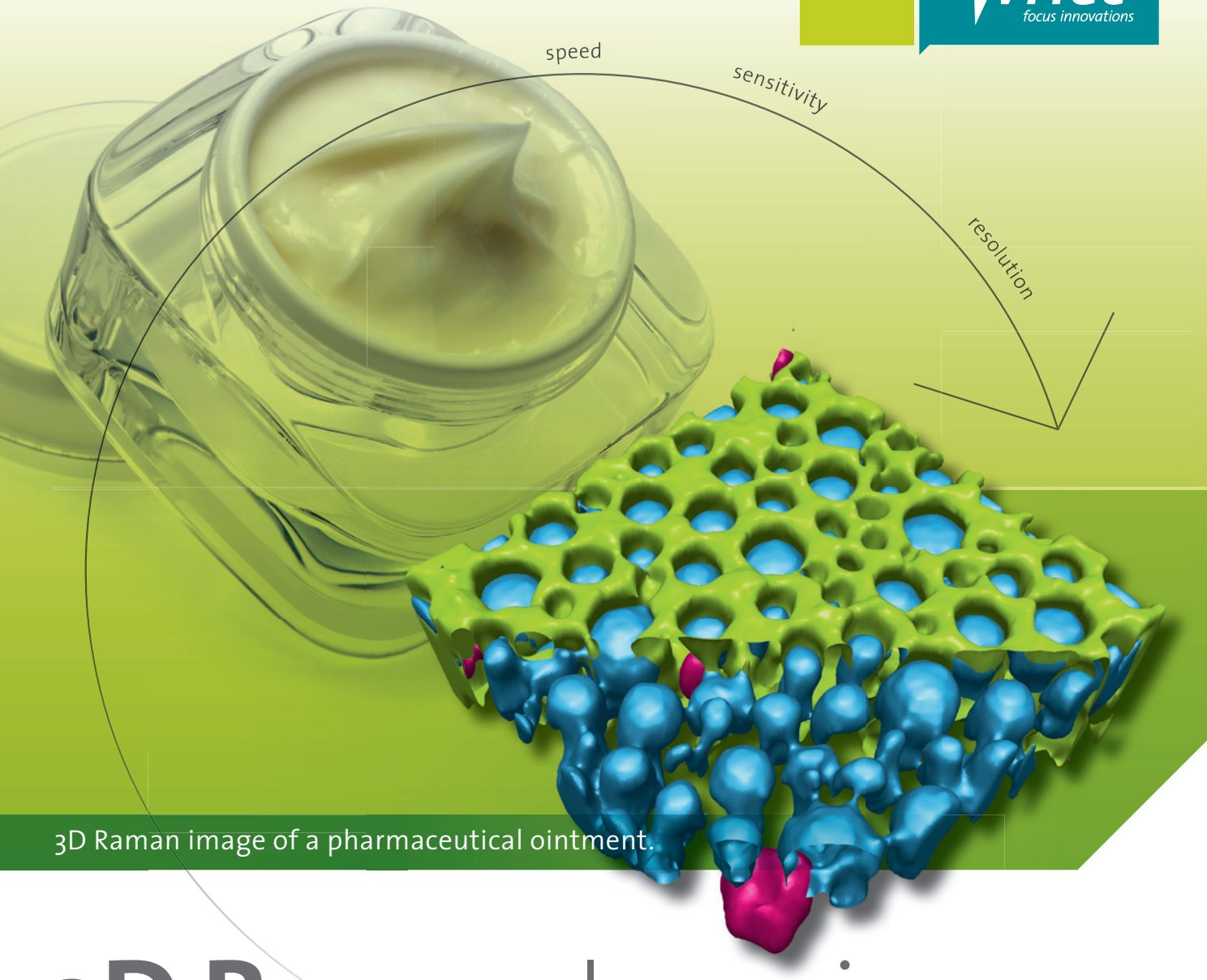

3D Raman image of a pharmaceutical ointment.

3D Raman Imaging

Turn ideas into **discoveries**

Let your discoveries lead the scientific future. Like no other system, WITec's confocal 3D Raman microscopes allow for cutting-edge chemical imaging and correlative microscopy with AFM, SNOM, SEM or Profilometry. Discuss your ideas with us at **info@witec.de.**

Raman · AFM · SNOM · RISE ***www.witec.de***

MADE IN **GERMANY**

KEY ELEMENTS OF CONFOCAL RAMAN MICROSCOPY FOR HIGH-RESOLUTION IMAGING

Thomas Dieing, Marius Henrich, and Sonja Breuninger

The sensitivity of a high-resolution Raman imaging system is crucial to the quality of the acquired information. The spectral and spatial resolutions are among the primary factors that influence the obtainable results. The limits of resolution are defined theoretically by the laws of physics, but are experimentally determined by the instrument parameters. In this article, the theoretical background and the possibilities in practical applications are discussed.

Confocal Raman microscopes are the instruments of choice for many Raman measurements in a wide variety of applications ranging from geosciences (1–3), biology (4–6), nanocarbon materials (7–9) to pharmaceutical compounds (10,11), just to name a few. This article sheds light on the possibilities and, in part, the origins in terms of spectral and spatial resolution for confocal Raman systems in general.

Spectral Resolution

Any confocal Raman system will have a spectral resolution which is mainly determined by the following parameters:

- the focal length of the spectrometer (the longer the focal length, the higher the spectral resolution)

- the grating (the higher the groove density, the higher the spectral resolution)
- the pixel size on the charge-coupled device (CCD) camera (the smaller the pixels, the higher the spectral resolution)
- the entrance slit or pinhole (the smaller the slit or pinhole the higher the spectral resolution)
- the line shape preservation (equals imaging quality) of the spectrometer.

In some cases, one of the parameters can put limitations on the spectral resolution. If, for example, the projection of the pinhole onto the CCD is already large compared to the pixel size on the CCD camera, then a further reduction of pixel size will not increase the spectral resolution.

Please note that the microscope components such as the objective used for collection of the signal should not influence the spectral resolution if the entrance slit or pinhole is the limiting element. This is preferential with confocal Raman microscopes.

The determination of the spectral resolution is often a point of debate. First, one should clearly differentiate the spectral resolution from the sensitivity of the system to detect shifts of individual peaks. Relative peak shifts can be detected with a much higher accuracy using fitting algorithms as has been demonstrated with a sensitivity down to 0.02 rel. 1/cm standard deviation of the peak shift of a Si peak (12). The maximum achievable fit accuracy depends heavily on the number of detected photons and the width of the peak that is fitted. This shift analysis is especially relevant for examining stress within a sample, but may not be taken as a measurement for the spectral resolution.

The spectral resolution, which determines how the system can measure (that is, full width at half maximum [FWHM] of a narrow peak or how well overlapping peaks can be differentiated), needs to be addressed separately from the peak shift sensitivity. There are various ways to state the spectral resolution, and some of the most common ones are outlined below.

Pixel Resolution

The *pixel resolution* is the difference in wavenumbers when moving from one pixel on the CCD camera to the next and is independent of factors such as slit width or peak width of the detected peak. This can only be seen as the true resolution limit if the pixel size and not the size of the entrance slit or pinhole is the limiting factor. For example, if the image of the slit or pinhole on the CCD camera is 100 μm in diameter and the pixel size on the CCD camera is 26 μm, then the resolution would be significantly worse than the distance (in wavenumbers) between two pixels. Since wavenumbers are measured in reciprocal space, it also needs to be noted that the pixel resolution will differ depending on the spectral position where it is

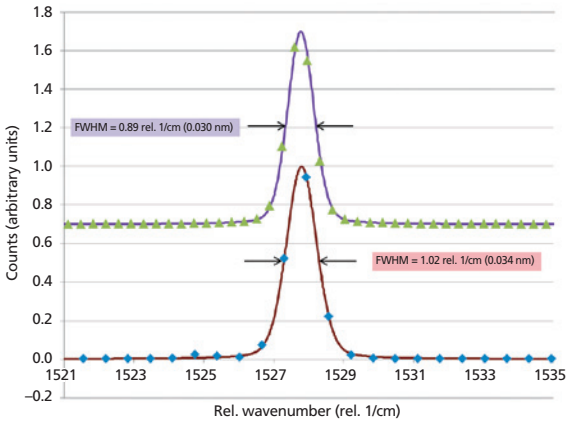

Figure 1: Spectra of the mercury atomic emission line at 579.066 nm plotted as a function of wavenumber assuming a 532.00-nm excitation. The red line is the fitted curve (pseudo voight function) and the blue diamonds are the measured data points for the 1800-grooves/mm grating. The green triangles and the purple curve show the results obtained using the 2400-grooves/mm grating.

determined. The resolution close to the Rayleigh line can, in this way, differ by almost a factor of two from the pixel resolution near 3500 rel. 1/cm in the case of 532-nm excitation.

Two-Pixel Criterion

For this criterion two times the pixel resolution is taken. The logic behind this is that to discriminate two neighboring peaks one needs to have one pixel on one peak, one in the minimum between the peaks, and a third one on the next peak. This criterion is analogous to the Nyquist theorem in signal processing. The same limitations as outlined for the pixel resolution criterion apply in this case.

Full Width at Half Maximum of Atomic Emission Lines

Atomic emission lines are typically much narrower than any Raman line. Their narrow width makes them a good probe to check the resolution. Figure 1 shows an atomic emission line of mercury near 579.07 nm. The *x*-axis is given in units of rel. 1/cm assuming a 532.00-nm excitation laser. The spectrum was recorded using a mercury and argon calibration lamp coupled via a 10-µm core diameter multimode fiber to a UHTS300 spectrograph (WITec GmbH) equipped with both 1800- and 2400 grooves/mm gratings (BLZ at 500 nm) and a Newton electron multiplying charge coupled device (EMCCD) camera with a pixel size of 16 µm. The integration time was 0.1 and 0.24 s, respectively, for the spectra. The FWHM derived through this approach is a good measure of the resolution, but care must be taken to ensure that enough points are available within the curve to ensure a good fit to the curve.

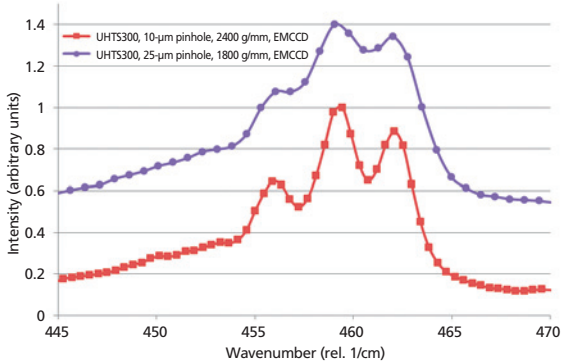

Figure 2: Raman spectrum of CCl_4 with 532-nm excitation at different spectral resolutions.

Measurement of Peak Resolution on Known Reference Samples

There are a few samples that are established standards to demonstrate spectral resolution. The most prominent is probably CCl_4. Figure 2 shows two spectra of this substance recorded with different spectral resolutions. It can clearly be seen, that the peaks are nicely separated in the red spectrum whereas the separation is not as clear for the purple spectrum.

Therefore, spectral resolution can be defined in many different ways and, thus, it is advisable to specify exactly how a spectral resolution was or should be determined. Comparing actual measurement results under identical measurement conditions is certainly one of the best ways to illustrate this. It should also be noted that with few exceptions the natural linewidths of Raman lines are typically larger than 3 rel. 1/cm. Taking the Nyquist criterion into consideration, a resolution in the range of 1 rel. 1/cm should be sufficient for the majority of samples.

Spatial Resolution

When considering the spatial resolution of a confocal Raman microscope one may distinguish between the lateral (*x* and *y*) resolution and the depth resolution. However, in either case, it is possible that the limitations arise because of one of the five following points:

- basic physics (that is, diffraction limit)
- limited positioning accuracy of the mechanical components used
- limitations because of the optical components used in the beam path (that is, beam distortion)
- nondiffraction limited sample illumination
- pixel resolution of the image acquired.

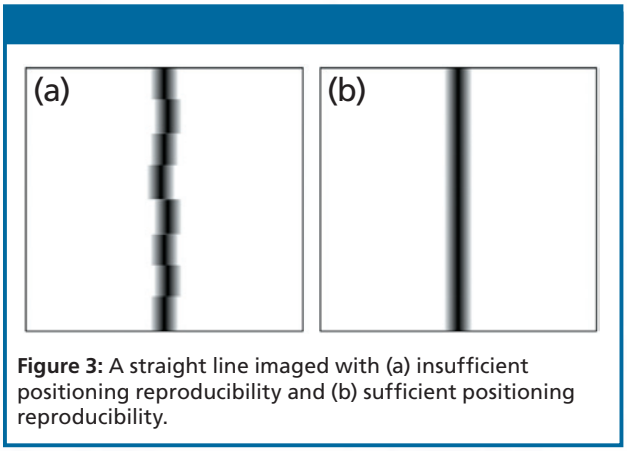

Figure 3: A straight line imaged with (a) insufficient positioning reproducibility and (b) sufficient positioning reproducibility.

In terms of the positioning system, it is important to differentiate the single step accuracy of a stepper motor, the positioning reproducibility, and linearity. The reproducibility and linearity are the key factors for an imaging system since this allows a line by line imaging. If, for example, a straight line is imaged, then this line will only be imaged with the accuracy of the positioning reproducibility even though the step size might be much smaller. Figure 3 illustrates this effect with Figure 3a showing insufficient positioning reproducibility and Figure 3b showing sufficiently high positioning reproducibility.

The necessary positioning reproducibility should therefore be several factors better than the smallest imaged object, or if the system should

allow the best physically possible resolution, several factors (that is, 10×) better than the diffraction limit.

Using high-quality components and positioning systems should allow imaging approaching the limits of physics.

Lateral Resolution

Based on the diffraction theory of Ernst Karl Abbe, Lord Rayleigh defined the diffraction limit in 1896. Rayleigh thereby quantified the minimal distance at which two point light sources can be identified. In this case, one of the sources is located at exactly the distance of the first minimum of the Airy function (point spread function) of the other one. This distance (d_{lim}) can be expressed as a function of the wavelength emitted (λ) and the numerical aperture (NA) of the objective used as:

$$d_{lim} = 0.61 \frac{\lambda}{NA} \quad [1]$$

The equation 1.22 λ/NA is often also found in this context, but this describes the distance between the two first minima of the Airy function and not the diffraction limit as described by Lord Rayleigh. Using the definitions of the Airy function the resolution can be easily derived by how much the intensity between the two emitting points has to decrease according to the Rayleigh criterion. Please note that the distance is different for other criteria of diffraction such as the Abbe criterion or the Sparrow criterion.

To derive the resolution of a microscope using either of those criteria it would be necessary to have a variety of very small, well scattering objects (small compared to the size of the Airy disk; for example individual TiO_2 particles) at varying distances. Following high-resolution Raman imaging, one would then have to analyze the signal intensities and based on the detectable distances between the spots one would have to derive the resolution.

An easier way to determine the lateral resolution power of a system uses the FWHM of small objects. Based on the Airy function the relation between the FWHM of the light emitted from an object and the diffraction limited distance (d_{lim}) is:

$$FWHM \approx 0.85\, d_{lim} = 0.51 \frac{\lambda}{NA} \quad [2]$$

Because the measured signal is always a convolution between the object size, the emission characteristics, and the system function, the objects measured in such experiments also have to be small compared to the Airy disk. Mathematically speaking, the object's size should approach a delta function for the convolution. Such small objects naturally have only limited material which scatters and thus one may expect small Raman signals emitted by them. Carbon nanotubes (CNTs) on the contrary show a large Raman signal while being very small in diameter (typically ranging from

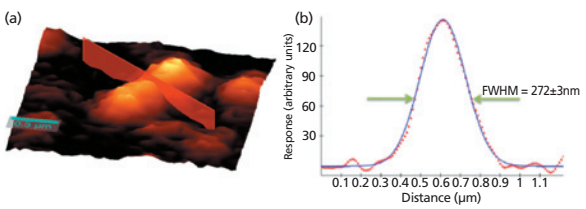

Figure 4: Integrated intensity of the G-band of a carbon nanotube with (a) the cross section position marked in red and (b) the cross-sectional intensity along this line. The lateral resolution of the microscope system can be characterized by the FWHM and is about 272 nm.

subnanometer to a few nanometer range) and comparatively long (up to a few micrometers typically). These samples are thus the ideal probes to check the lateral resolution of a confocal Raman microscope. For a 532 nm excitation laser and an objective with an numerical aperture (NA) of 0.9 one should therefore be able to obtain a FWHM across CNTs of about 301 nm.

Figure 4a shows the integrated intensity of the G-band on a sample of CNTs on a Si substrate. The scan range was 1.5 µm × 1.5 µm with 50 × 50 points and an integration time of 23 ms per point was used. An alpha300R system (WITec GmbH) was used for the measurement in combination with a fiber-coupled, frequency-doubled Nd:YAG laser (532 nm emission), a Zeiss 100× NA 0.9 objective, and a 50-µm multimode fiber acting as the pinhole for confocal microscopy. For this microscope and objective this corresponds to a projected pinhole size of 500 nm in the focal plane. The spectrometer used was a UHTS300 (WITec GmbH) with a 600-grooves/mm grating (BLZ at 500 nm) combined with a back-illuminated CCD camera.

The red line in Figure 4a indicates where the cross section shown in Figure 4b was extracted from. It can clearly be seen that the FWHM is even narrower than the predicted minimum.

The theory of confocal microscopy (for example, see reference 13) shows that the achievable resolution can further be decreased by a maximum of $1/\sqrt{2}$. In confocal Raman microscopy this fact is rarely used to its limit, because it requires a strong reduction of the pinhole diameter, which in turn reduces the throughput.

Depth Resolution

Depth resolution is the best proof of the confocality of a system. The instrument design has a key influence on the achievable resolution, but the pinhole or slit as well as the way the sample is illuminated also play a crucial role for the depth resolution. Therefore, these points are outlined below before the physical limit of the depth resolution is discussed.

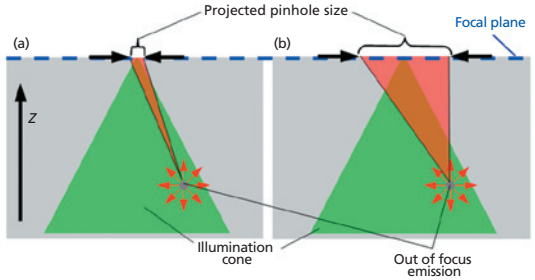

Figure 5: The light collected from an out of focus emitter through the projected pinhole and thus the physical pinhole for the case of (a) a small pinhole and (b) a large pinhole or slit.

Pinhole or Slit

The pinhole plays a crucial role for the depth resolution in confocal microscopy. However, the physical size of the pinhole ($P_{physical}$) cannot easily be compared between different instruments. In image generation using two simple lenses, the focal length of both lenses contributes to the ratio between the object and the image size. This of course also holds true for a microscope. Here, we have the magnification of the objective ($M_{Objective}$), which is calculated for a certain focal length of the tube or telan lens ($f_{Tube, Objective}$). This focal length ranges for commercial microscopes from 164.5 mm for Zeiss objectives up to 200 mm for Leica or Nikon objectives. The magnification printed on the objective is only correct if the objective is designed for the tube focal length of the microscope. To have a comparable value for the pinhole size one should therefore calculate the projected pinhole size (P_{proj}) as follows:

$$P_{proj} = \frac{P_{physical}}{M_{eff}} = \frac{P_{physical}}{M_{Objective}\frac{f_{Tube, Objective}}{f_{Tube, real}}} \quad [3]$$

The same calculation also applies if a slit is used as a pinhole. For the following considerations, we will use the projected pinhole instead of the physical pinhole size.

The influence of the projected pinhole size is illustrated in Figure 5. Here, a point illumination of a small area with an objective with a relatively high NA value is assumed. The collection diameter of the objective is assumed to be larger than the area shown and, thus, this is assumed not to be the limiting factor here.

If the sample is transparent enough, the light will propagate further through the sample beyond the focal plane as shown by the illumination cone in Figure 5. This light can excite out-of-focus molecules, which can then emit light (Rayleigh, fluorescence, Raman, and so on) in turn. This emission is isotropic, so part of the light will find its way through the position of the projected pinhole in the focal plane and, thus, also through the physical pinhole. When comparing Figures 5a and 5b, it is apparent that a large pinhole allows a much higher amount of out of focus light to be detected. Therefore, a larger pinhole as well as a slit can never achieve the same suppression of out of focus light compared to a small pinhole.

Sample Illumination

In the last section it was shown that part of the emission from out-of-focus material will always pass through the pinhole and that the contribution of this emission to the detected signal is highly dependent on the pinhole size. The intensity of the excitation light at such an out-of-focus position is, in addition, directly proportional to the emitted light. This intensity is decreasing with an increasing distance of the point from the focal plane. The strength of this decrease, however, is

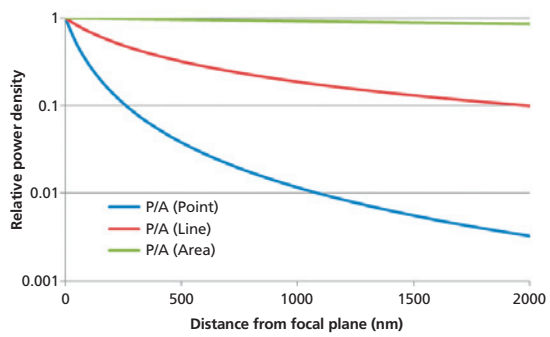

Figure 6: Relative laser power density as a function of distance from the focal plane.

heavily dependent on the way the sample is illuminated and can best be compared by taking the power density (power or area) into consideration. Given a fixed illumination power, one can simply take the increase in the illuminated area as a function of depth into consideration. The numerical aperture of the objective is essential in this consideration. The higher the numerical aperture, the faster the increase of the area as a function of depth and, thus, the faster the decrease of the power density as a function of depth. In addition to the numerical aperture, the way the sample is illuminated plays a key role. Global illumination shows the smallest decrease as a function of depth. Line illumination shows a faster decrease and point illumination gives the fastest decrease of the laser power density as a function of depth (see Figure 6). For the example shown, a point focus of 0.5 µm diameter, a line focus of 1 µm × 100 µm, and a global illumination of 100 µm diameter was used. The NA value used for the calculations was 0.9. For this approximation, a truncated cone was used as the geometry of the point and global illumination and a truncated pyramid were used for the line illumination.

Real-world samples have additional absorption of the laser power as a function of depth, but this would affect all three curves similarly.

Thus, when comparing point illumination with a confocal pinhole and line illumination with a slit, it is apparent that more light of the out-of-focus emitters passes through the pinhole (see Figure 5) and, in addition, the power density in these out of focus planes is significantly higher (in the example shown in Figure 6 it is a factor of ~16 at a 1000-nm depth). The depth resolution achievable with line or global illumination cannot achieve the same values as point illumination. All of the following considerations are therefore calculated and measured for a point illumination and a circular pinhole.

Theory and Measurement of Depth Resolution

For the prediction of the possible depth resolution in confocal Raman microscopy one commonly uses the theory applicable for small numerical apertures (for example see reference 13). This theory predicts a minimal achievable FWHM in the z-direction (at minimal pinhole diameter) of about 940 nm for a 532-nm laser and a 0.9-NA objective.

To probe this depth resolution one can

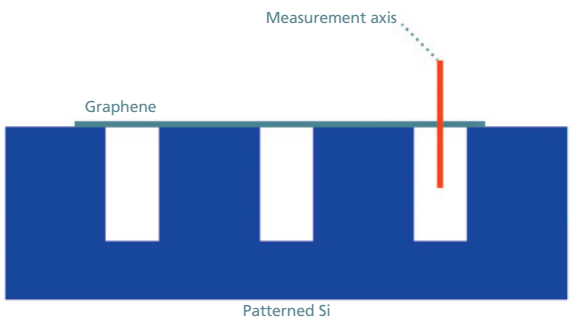

Figure 7: Graphene is suspended over holes in Si to determine the depth resolution. The red line displays the measuring position.

perform a depth scan on silicon (Si), which shows a very small penetration depth for 532-nm excitation, is available in virtually every laboratory, and has a strong Raman signal. Following the discussion outlined for the lateral resolution, however, a very thin sample would be ideal. Graphene or ultrathin graphite (that is, 5–10 atomic layers) suspended over holes in Si is an ideal sample to illustrate this (see Figure 7 for a schematic of the sample). Similar to the CNTs for the lateral resolution, graphene has a very strong Raman signal and can act as an approximation for a delta function for the convolution of the sample geometry with the system function.

Figure 8a shows a depth profile of the integrated intensity of the first order Si peak (red) and the integrated intensity of the peak near 1600 rel. 1/cm recorded on suspended ultrathin graphite. The system used was an alpha300R microscope (WITec GmbH) with a 100× NA 0.9 Zeiss objective, a 10-µm pinhole (100 nm projected pinhole diameter), and a UHTS300 spectrometer (WITec GmbH). The integration time per point was 2 s and the step width was 50 nm. The *z*-position was set by an interferrometrically calibrated piezoelectric positioning table. The depth profiles in Figure 8a are offset for clarity. Figure 8b shows the spectrum of the ultrathin graphite in focus with a 2-s integration time.

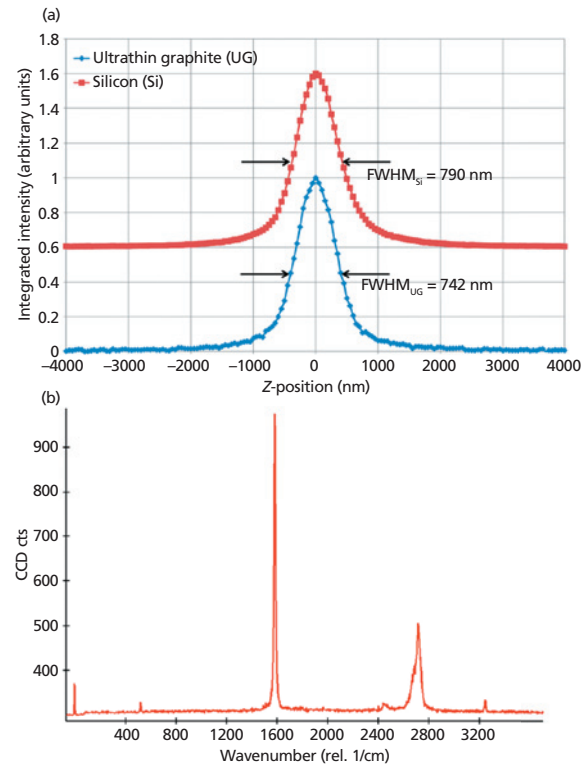

Figure 8: (a) Depth profile on suspended ultrathin graphite and Si. (b) A single spectrum on suspended ultrathin graphite (integration time 2 s).

A close comparison of the depth profile of Si with the one collected from ultrathin graphite shows that the rising part of the curve (negative *z*-position values; above the sample surface) are virtually identical.

The falling half (positive *z*-position values; below the sample surface) shows a broadening for the Si curve. This broadening is because of the penetration of the laser into Si. This penetration depth is small for a green laser and Si, but would be considerably more for a near-IR laser and, thus, the curve of Si would be further distorted on the falling half. For excitation using a green laser source this comparison shows, however, that the commonly available Si can be used as a very good probe to obtain information on the depth resolution of a system.

Comparing these results to the theory for low numerical apertures illustrates that it cannot be valid for high numerical apertures. Converting this theory to match the high numerical aperture case is not trivial, but an approximation can be given following the work by Mack (14). Based on this, the ratio between the low numerical aperture and the high numerical aperture results can be calculated as

$$\frac{\text{low NA result}}{\text{high NA result}} = \frac{4\sin^2\left(\frac{\Theta}{2}\right)}{\sin^2(\Theta)} \quad [4]$$

where θ is half of the opening angle of the objective. For an NA value of 0.9 this results in a correction factor of 1.38. Thus, the best depth resolution achievable according to this approximation should be about 682 nm.

The work by Wilhelm and colleagues (15) for confocal laser scanning microscopy can also be followed for this purpose. From this we find an axial optical resolution dependent on the projected pinhole size. For projected pinhole sizes larger than one "Airy unit" (1.22*λ/NA) the following equation applies:

$$FWHM_{axial} = \sqrt{\left(\frac{0.88 \cdot \lambda_{em}}{\left(n - \sqrt{n^2 - NA^2}\right)}\right)^2 + \left(\frac{\sqrt{2} \cdot n \cdot P_{proj}}{NA}\right)^2} \quad [5]$$

where λ_{em} refers to the emitted wavelength. Using the experimental parameters shown above with λ_{em} = 580.7 nm, this results in an axial FWHM of 920 nm. It should be noted however, that the projected pinhole size is significantly smaller than the Airy unit in the presented data. For this case, the work by Wilhelm (15) suggests a different equation as follows:

$$FWHM_{axial} = \frac{0.64 \cdot \bar{\lambda}}{\left(n - \sqrt{n^2 - NA^2}\right)} \text{ with } \bar{\lambda} = \sqrt{2}\,\frac{\lambda_{em} \cdot \lambda_{exc}}{\sqrt{\lambda^2_{exc} + \lambda^2_{em}}} \quad [6]$$

With this, the calculated result is about 630 nm FWHM.

These theories do not result in the same axial resolution, which clearly indicates that there are some inconsistencies in the calculations (that is, between equations 4 and 6). It can however, clearly be seen both from the theories as well as experimentally, that FWHMs well below 1 μm are possible and can be expected from confocal Raman microscopes.

Summary

Confocal Raman microscopes allow the measurement of nanometer-size objects and, using such objects, the spatial resolution of the systems can be easily

determined. The experimental results that are routinely achieved are very close to the theoretical predictions. The spectral resolution needs to be clearly defined and standard samples or light sources are best used to determine this. A reliable comparison should ideally duplicate all relevant parameters and, for example, require all resolution measurements to be performed using the same projected pinhole size.

References

(1) P. Jenniskens, M.H. Shaddad, D. Numan, S. Elsir, A.M. Kudoda, M.E. Zolensky, L. Le, G.A. Robinson, J.M. Friedrich, D. Rumble, A. Steele, S.R. Chesley, A. Fitzsimmons, S. Duddy, H.H. Hsieh, G. Ramsay, P.G. Brown, W.N. Edwards, E. Tagliaferri, M.B. Boslough, R.E. Spalding, R. Dantowitz, M. Kozubal, P. Pravec, J. Borovicka, Z. Charvat, J. Vaubaillon, J. Kuiper, J. Albers, J.L. Bishop, R.L. Mancinelli, S.A. Sandford, S.N. Milam, M. Nuevo, and S.P. Worden, *Nature* **458**, 485–488 (2009).

(2) A. Rotundi, G.A. Baratta, J. Borg, J.R. Brucato, H. Busemann, L. Colangeli, L. D'Hendecourt, Z. Djouadi, G. Ferrini, I.A. Franchi, M. Fries, F. Grossemy, L.P. Keller, V. Mennella, K. Nakamura, L.R. Nittler, M.E. Palumbo, S.A. Sandford, A. Steele, and B. Wopenka, *Meteorit. Planet. Sci.* **43**, 367–397 (2008).

(3) C. Heim, J. Lausmaa, P. Sjovall, J. Toporski, T. Dieing, K. Simon, B.T. Hansen, A. Kronz, G. Arp, J. Reitner, and V. Thiel, *Geobiology* **10**, 280–297 (2012).

(4) S. Hild, F. Neues, N. Znidarsic, J. Strus, M. Epple, O. Marti, and A. Ziegler, *J. Struct. Biol.* **168**, 426–436 (2009).

(5) N. Gierlinger and M. Schwanninger, *Spectroscopy* **21**, 69–89 (2007).

(6) A. Hermelink, A. Brauer, P. Lasch, and D. Naumann, *Analyst* **134**, 1149–1153 (2009).

(7) Y.N. Xu, D. Zhan, L. Liu, H. Suo, Z.H. Ni, T.T. Nguyen, C. Zhao, and Z.X. Shen, *ACS nano* **5**, 147–152 (2011).

(8) Y. You, T. Yu, J. Kasim, H. Song, X. Fan, Z. Ni, L. Cao, H. Jiang, D. Shen, J. Kuo, and Z. Shen, *Appl. Phys. Lett.* **93**, 103–111 (2008).

(9) T. Yu, Z. Ni, C. Du, Y. You, Y. Wang, and Z. Shen, *J. Phys. Chem. C* **112**, 12602–12605 (2008).

(10) C. Matthaus, A. Kale, T. Chernenko, V. Torchilin, and M. Diem, *Mol. Pharm.* **5**, 287–293 (2008).

(11) T. Chernenko, C. Matthaus, L. Milane, L. Quintero, M. Amiji, and M. Diem, *ACS nano* **3**, 3552–3559 (2009).

(12) http://www.witec.de/en/download/Raman/StressinSi.pdf.

(13) T. Dieing, O. Hollricher, and J. Toporski, *Confocal Raman Microscopy,* (Springer, 2010) ISBN 978-3-642-12521-8.

(14) C.A. Mack, *Microlithogr. World,* February edition, 14–15 (2004).

(15) S. Wilhelm, B. Gröbler, M. Gluch, and H. Heinz, Confocal Laser Scanning Microscopy, http://zeiss-campus.magnet.fsu.edu/referencelibrary/pdfs/ZeissConfocalPrinciples.pdf.

Thomas Dieing, PhD, Marius Henrich, and Sonja Breuninger, PhD, are with WITec GmbH in Ulm, Germany. Direct correspondence to: sonja.breuninger@witec.de

This article originally appeared in *Spectroscopy*, **29** (S6), (2014), 42–54. ■

ANALYSIS OF THE STATE OF THE ART: RAMAN SPECTROSCOPY

Megan L'Heureux

Spectroscopy asked a panel of experts to assess the current state of the art of Raman spectroscopy and to try to predict how the technology will develop in the future.

Sir C.V. Raman discovered Raman spectroscopy in the late 1920s, which is where the nomenclature comes from (1). In the eight decades since that discovery, Raman spectroscopy has had plenty of time to mature, yet users continue to find new application areas for the technique. *Spectroscopy* recently asked a panel of Raman experts about the current state of Raman spectroscopy—including the various advanced subsets of Raman such as stimulated Raman scattering (SRS), coherent anti-Stokes Raman scattering (CARS), and tip enhanced Raman scattering (TERS)—including recent advances, ongoing challenges, and possible future developments. This article is part of a special group of six articles covering the state of the art of key techniques, also including infrared (IR) spectroscopy, near-infrared (NIR) spectroscopy, inductively coupled plasma–mass spectrometry (ICP-MS), laser-induced breakdown spectroscopy (LIBS), and X-ray fluorescence spectroscopy.

Recent Advances

We started by asking our experts what they considered the most important development in Raman spectroscopy or its instrumentation in the last 5–10 years. The answers covered a variety of advances and specialized application areas, making it clear that Raman continues to break through its limitations and find new ways to support the fields of research and industries where it is used.

Dennis J. Walls, a senior research associate at DuPont, is excited about the progress in SRS and CARS that has made Raman imaging more practical in terms of speed and applicability. "Developments in coherent Raman scattering microscopy approaches such as SRS and CARS microscopy offer exciting potential in biological imaging applications," Walls said. He also mentioned the importance of TERS. "I also am excited about the potential for sub-diffraction limited microscopic approaches like TERS, which are now crossing boundaries of spatial resolution that have previously not been accessible with normal Raman microscopy."

Zachary D. Schultz, an associate professor of chemistry and biochemistry at the University of Notre Dame, agrees that TERS is an important development. "The understanding of the relationship between plasmon resonances and Raman signal enhancements has rapidly advanced in the last decade," Schultz said. "This is evident in the increased interest in surface-enhanced Raman scattering (SERS) for applications and the emergence of TERS for sub-diffraction imaging." Schultz explained that recent work has taken advantage of this understanding, demonstrating the reproducibility and quantitative capabilities of SERS and TERS. "It is really becoming possible to talk about using Raman to investigate individual molecules," Schultz concluded.

Heinz W. Siesler, a professor at the University of Duisburg-Essen, said that handheld Raman was the most important recent advance. Gary Johnson, a research Chemist at Intertek, agreed. "I am very interested in the development of compact, portable instruments that have the capability to obtain spectra equivalent to the performance of benchtop systems," Johnson said. This is valuable, he said, because there are a lot of potential applications of Raman spectroscopy for which it is impractical to bring samples into a laboratory.

John A. Reffner, a professor at John Jay College of Criminal Justice in New York, said that solid-state lasers and the development and application of optical filters for Rayleigh scattering rejection have had the greatest impact on Raman instrumentation.

From a different perspective, Juergen Popp, a professor of physical chemistry at Friedrich-Schiller University Jena and the Leibniz Institute of Photonic Technology Jena, said that the most important recent advances have been developments in instrumentation that have pushed Raman spectroscopy further into life sciences and biomedicine. "This development

was certainly triggered by the technical progress made in spectrometer, detector (charge-coupled device [CCD]), and filter (notch filter) technology," said Popp. "These technological advancements made Raman spectroscopy accessible for a broad circle of users because of the availability of commercially available and fairly easy-to-use Raman setups, in particular, confocal Raman microscopes." The availability of confocal Raman microscopes allowed for label-free molecular characterization of biological cells and tissue with a spatial resolution in the submicrometer range, he said. "This paved the way for medical Raman spectroscopy, that is, Raman spectroscopic clinical diagnosis," he said.

These advances wouldn't have been possible, he noted, without the simultaneous achievements in statistical Raman data analysis—that is, the development of innovative chemometric strategies to analyze Raman spectra of biological specimens. "In other words, I consider the development of innovative chemometric approaches to qualitatively and quantitatively analyze Raman images with respect to utilizing the Raman signatures for diagnostic purposes as one of the most important aspects in biomedical Raman spectroscopy," he said.

Fluorescence Background Response

Despite these important advances, however, fluorescence background response still limits the use of Raman spectroscopy for many applications of

interest. In light of this, we asked our panel the following questions: How much of a problem is this in your work? What tools do you have to eliminate it? Are there any additional developments anticipated that could lead to significant improvements in dealing with this problem in the near future?

Common Problem

All of our panelists agreed that fluorescence is a common problem in their work. Walls said that fluorescence is one of the "major factors that limits applications for Raman spectroscopy" to the varied analyses that come through his laboratory.

Reffner agreed. "Fluorescence creates an uncertainty that limits the reliability of using Raman for analysis of some samples," he said.

Johnson said he runs into this problem frequently, particularly with industrial samples and materials that contain natural products. Schultz agreed that background signals are still a problem. "In SERS and TERS, the metals often provide some fluorescence quenching, but molecules distant from the nanostructures can still cause problems," said Schultz.

Tools to Eliminate Fluorescence

Most of our panelists said they use excitation wavelength selection to mitigate the problem of fluorescence.

Popp's main focus lies in the application of Raman spectroscopic approaches for biomedical diagnosis, so he primarily uses excitation wavelengths in the NIR region (mostly 785 nm) to avoid the excitation of fluorescence. Siesler agreed that NIR excitation is the best approach. "The recently patented sequentially shifted excitation (SSE) technique (2) might possibly help to suppress fluorescence, but I have not had the opportunity to test it yet," he said.

Walls said that he also uses NIR excitation at 785 nm to avoid fluorescence, but even then, many classes of samples remain outside of the scope of application for Raman spectroscopy because of fluorescence background issues. "Alternatively, excitation at 1064 nm can address some of these samples," he said.

Another approach that Popp's laboratory is pursuing is the use of excitation wavelengths in the deep ultraviolet (UV) at 244 nm. "The application of deep UV wavelengths also avoids fluorescence since most fluorophores do not show fluorescence below 250 nm," he said. He noted that this deep UV approach is especially powerful for mineralogical studies. "Furthermore, I think shifted excitation Raman difference spectroscopy is a powerful approach to eliminate fluorescence."

Johnson mentioned photobleaching as an alternative that is sometimes effective, but otherwise he agreed that 785-nm or near-infrared 1064-nm lasers were the best tools to eliminate the fluorescence problem.

Finally, Reffner said that SERS is showing "real progress in reducing the

fluorescence problem while amplifying the Raman scattering."

Potential Future Solutions

A few of our panelists suggested some future developments that might help to solve the fluorescence interference problem. Schultz explained one possible approach: rapidly switching the laser frequency over a small wavelength range. This technique would change the Raman signal but not the fluorescence. "Incorporating this or similar ideas into commercial instruments may resolve the fluorescence background problem at some future time," he said. He added that the advent of NIR cameras and array detectors makes Raman possible with excitation wavelengths that do not cause fluorescence. "These new technologies are helping to resolve this problem," Schultz concluded.

Walls said that continued advances in the incorporation of the 1064-nm excitation source in dispersive instruments would allow practical data collection (from the standpoints of time and laser power) and would be an important advance.

Popp said that a technical improvement to avoid fluorescence interference could be the development of fast detectors to separate fluorescence and Raman scattering in time. "One example of this is superconducting nanowire single-photon detectors" he said.

Biomedical Applications

Recent reports of the successful use of Raman spectroscopy for important biomedical applications are quite exciting. These applications include imaging for disease diagnosis, including significant improvements for endoscopic probes, and identification of microorganisms. We asked our panelists for their opinions about the practicality of implementing these technologies in the clinical environment.

Siesler said that the implementation of these technologies as routine tools would likely be very slow. "The promises in various ads are too optimistic," he said.

Popp had a more positive outlook on the work being done in this area, which is the focus of his research group. He has observed an enormous increase in the development and application of Raman-based approaches to address biomedical questions. "The ability to obtain specific chemical information label-free makes Raman spectroscopy attractive for many applications in clinical diagnostics of bodily fluids, pathogens, cells, and tissue biopsies," he said. "I am absolutely convinced that Raman spectroscopy might be the solution for many clinical challenges that have unmet medical needs, for example, in the early detection of cancer."

As another example, Popp mentioned the significant progress made toward the application of Raman spectroscopy as a point-of-care test for the fast identification of pathogens (such as sepsis-causing

pathogens) and the determination of their antibiotic resistances. "Overall, I am sure that a few years from now we will see the first Raman approaches as standard diagnostic or therapeutic tools in daily clinical practice," he said.

Schultz agrees that nonlinear Raman techniques have a lot of potential in the biomedical imaging community. "The label-free, video-rate images that are obtainable may have a tremendous impact on identifying cancerous tissue or other abnormalities," he said.

"In respect to identifying microorganisms, rapid assays based on SERS are really starting to make an impact," Schultz said. He explained that applications identifying tuberculosis, flu viruses, and other pathogens have all been demonstrated already. "Handheld Raman instrumentation may make these assays highly portable and inexpensive," he said. Schultz also said that work with high-throughput detection with moving fluids, such as chromatography, flow injection analysis, and microfluidic approaches, is another important advance for clinical environments. "I think Raman has an important future in the biomedical community," he concluded.

Johnson added a caution, however, noting that the primary challenge in applying Raman to clinical use lies in data analysis and interpretation. "Considerable care is needed to avoid misdiagnosis, especially when using chemometric methods that don't rely on well-defined spectral features," he said.

TERS

Many problems at the frontiers of materials science require spatial resolution that is outside of the diffraction-limited regime. Sub-diffraction-limited approaches like TERS seem to offer the potential to bridge this gap, but currently the approach does not appear to be practical because of the difficulty in preparing tips. So we asked our panelists if they thought TERS-like approaches to Raman imaging would someday become more practical.

"This remains an important opportunity for Raman spectroscopy that could be put to work today with practical instrumentation offerings and a ready source of appropriate tips," said Walls. "In addition to biological systems, the increasing importance of structural organization at the nanoscale in materials science calls for characterization approaches that can operate in this size regime."

Schultz said he was not sure if the difficulty is really preparing tips. "I think the biggest obstacle to TERS is false expectations," he said. "Many TERS tips perform exactly as expected; however, the observed signal enhancement from a single nanostructure on a single or small number of molecules, or in complex samples, is not always that large."

Schultz added that the advances

in commercial TERS instruments is helping practicality, but also increasing frustration when people cannot get the expected result. "I think TERS has significant potential and will be an important technique, but it will also have its limitations," Schultz said. "As the technique matures, people will better appreciate what it can and cannot do."

Popp mentioned several examples that show how TERS-like approaches are becoming more practical, such as in the characterization of single viruses and in protein analysis. "TERS has made a lot of progress within the last few years, especially with respect to practical life science or biomedical applications," he said. "I am convinced that the difficulties in preparing reproducible TERS tips will be overcome soon."

SERS

SERS approaches offer the potential to increase the sensitivity of Raman spectroscopy in a wide range of systems. We asked our panel if SERS-based solutions have become easier for nonexperts to apply, and whether SERS is likely to become more universally applicable in the near future.

All agreed that the lack of reproducible substrates—and having them commercially available—is the biggest obstacle to more widespread use of SERS.

"One commercial supplier recently discontinued a SERS substrate product," lamented Schultz. "A few other products have emerged as possibilities, but the development of a robust high-enhancement substrate would facilitate use by nonexperts," he said.

Siesler agreed. "Once commercial substrates are available, SERS will become more universally applicable."

Several panelists noted that there are many efforts underway to try to address this challenge. "Recent advances in producing colloids with reproducible size and morphology are helping to address this problem," said Reffner.

Popp agreed. "One of the most promising approaches in my opinion is the usage of colloidal silver or gold nanoparticles, which are easy to prepare together with microfluidic chips," he said.

Despite the reproducibility problem, Popp thinks that lab-on-a-chip SERS concepts are very promising, particularly for drug and metabolite monitoring. "The routine analytical application of SERS comes down to the availability of reproducible SERS substrates," he said. "Once such SERS substrates are available, SERS-based solutions will be easy to apply—even for nonexperts—making them universally applicable."

Johnson is less optimistic. "I see SERS as a method that works well for very specific types of samples, but not so much as a general analytical technique," he said.

New Areas for Raman: Applications and Challenges

Most people consider Raman

spectroscopy a mature technique, but it is still being applied to new areas—in addition to fields like clinical diagnoses and medical imaging discussed above. So we asked our panel what new applications are emerging for Raman and what challenges are involved with those applications.

New Application Areas

New application areas for Raman spectroscopy range from art conservation, forensics, and homeland security, to nutrition, health, and agriculture.

Reffner said that a growing segment of Raman applications resides in field-portable Raman spectrometers, which are currently being used in homeland security and forensic applications.

Schultz also mentioned the increased use of Raman in the forensics field. "I think Raman will continue to see increased use in applications where the samples are sensitive to chemical modification," he said. "The art community has seen increasing use of Raman for restoration, conservation, and forgery detection."

Schultz also explained that advances in Raman instrumentation are making it a highly affordable method. "Mass spectrometry (MS) may still provide better absolute molecular identification, but Raman is holding its own and seems to provide complementary information where MS has trouble," he said.

Walls would like to see the role of Raman spectroscopy expand for applications in high growth areas like industrial biosciences, nutrition, and health. "One example is our interest in expanding the role of Raman microscopy in the analysis of agricultural plant systems to support the development of crop protection chemicals," he said. "A key attribute needed will be the sensitivity to detect low levels of the analytes of interest in complex (and potentially fluorescent) backgrounds. Ideally, these measurements would be performed without disturbing the viability of the plant."

Popp believes that Raman is one of the most important spectroscopic methods. "In my view, it is not exaggerated to say that Raman spectroscopy has become an indispensable analytical method for an extremely broad area of applications," he said.

Application Challenges and How to Overcome Them

Even though Popp considers Raman a rather mature technique, he still believes it faces challenges. "The great challenge faced in using linear Raman spectroscopy for almost all applications is its intrinsically low scattering cross section—that is, low sensitivity very often leading to rather long acquisition times," he said.

Techniques like SERS, resonance Raman, and nonlinear Raman effects like CARS or SRS try to address this problem by enhancing the Raman signal. "These nonlinear Raman approaches have seen a

renaissance mainly because of the recent progress made in the development of high intensive ultrashort laser sources," said Popp. "The implementation of these nonlinear Raman phenomena in laser scanning microscopes has resulted in powerful biomedical imaging approaches that show great potential to complement established clinical pathological diagnostic tools."

Schutlz believes that biggest challenge for Raman lies in creating large databases of reference spectra that can be searched to identify molecules, as can be done today with gas chromatography (GC)–MS. "The challenge here is still the variances between spectra with different SERS strategies, and there is currently some debate about TERS signals," he said. "If this can be resolved, I think Raman could compete with GC–MS characterization."

The challenges that Walls foresees in areas like industrial biosciences, nutrition, and health applications include fluorescence, sensitivity, and the ability to differentiate a meaningful analyte signal from a complex background response.

Automation or Spectral Processing

Next we asked our experts what types of new automation or spectral processing could help in their work. The majority of answers addressed software improvements.

Johnson would like to see the integration of image analysis routines into Raman instrument software that is used for mapping applications. "Particle count and size distribution as well as more sophisticated three-dimensional (3D) imaging applications would be beneficial too," he said.

Walls touched upon the need for libraries, similar to what Schultz cited as a main challenge earlier. "For those of us who use Raman spectroscopy for the identification of unknown species, the availability of larger, more-comprehensive electronic libraries would significantly impact the effectiveness of these efforts," he said. Most vendors are starting to incorporate chemometrics data reduction approaches within their software, he said, and the continued expansion of these efforts will be helpful in his work.

Looking to the Future

Finally, we asked our experts what future developments in Raman spectroscopy or its instrumentation can be expected in the coming years.

According to Schultz, SRS is an area that should be watched closely in the next few years, because the sensitivity associated with this nonlinear technique is impressive. There are still instrumentation challenges with this technique, however. "In SRS, you have to measure the difference in the laser intensity at the Raman frequency of interest before and after the sample, which typically requires expensive lock-in amplifiers and stable laser sources," he said. "This also often limits the spectral range and resolution." A potential solution, he suggested, would be a lock-in array detector. "If we

had lock-in arrays with 1024 channels like modern array detectors used for Raman, SRS may provide some additional advances," he concluded.

Popp thinks that the greatest potential for Raman lies in medical diagnostics. A key next step, he explained, is transferring Raman spectroscopy from *ex vivo* to *in vivo* applications by implementing Raman spectroscopy into endoscopic setups. "In this context, within the next few years we will see the development of various other novel Raman fiber probes for in vivo tissue screening of internal organs like the colon, stomach, or aorta," he said. "These developments will utilize advances in fiber technology (for example, fiber Bragg gratings, waveguide optics, and imaging fiber arrays) and easy-to-operate fiber laser approaches."

Reffner said that the advantage of Raman spectroscopy to record low energy rotational and vibration spectra is a promising area to develop.

The future development of capable, less expensive, and even portable instrumentation piques Walls's interest. With continued refinement and technology advances, he said, these developments will foster growth into new applications across a wide range of application areas. "These developments, along with more powerful 'expert user' driven software interfaces, will catalyze the growth of Raman technology into the hands of nonspecialists in spectroscopy in an increasingly diverse range of technical applications," he predicted.

Conclusion

Raman spectroscopy is an invaluable technique for a wide array of application areas. It's safe to say that this technique has a strong foothold on the future, no matter what new application areas come its way.

Acknowledgments

I would like to extend a special thank you to Fran Adar of Horiba and Dennis J. Walls of Dupont for their assistance with the questions and panelist recommendations.

References

(1) http://en.wikipedia.org/wiki/Raman_spectroscopy
(2) J. Cooper, M.F. Abdelkader, and K. Wise, US patent 8,570,507 B1, 29 October 2013.

Megan L'Heureux is the managing editor of *Spectroscopy* magazine.

This article originally appeared in *Spectroscopy,* **30** (6), 44–49 (2015). ■

WITec
focus innovations

3D Raman image of pollen and sugar crystals in honey.

3D Raman Imaging

Turn ideas into **discoveries**

Let your discoveries lead the scientific future. Like no other system, WITec's confocal 3D Raman microscopes allow for cutting-edge chemical imaging and correlative microscopy with AFM, SNOM, SEM or Profilometry. Discuss your ideas with us at **info@witec.de.**

Raman · AFM · SNOM · RISE

www.witec.de

MADE IN **GERMANY**

NOVEL APPLICATION OF RAMAN SPECTROSCOPY IN BIOPRESERVATION

A Q&A with Nilay Chakraborty

As cell-based therapies are increasingly investigated as potential cures for everything from cancer to immune system disorders, techniques that can detect and prevent damage to mammalian cells during preservation and long-term storage are critical.

Spectroscopy recently spoke with Nilay Chakraborty, PhD, MBA, an assistant professor in the department of mechanical engineering at the University of Michigan, Dearborn, whose research focuses on developing new techniques for improving the survival of mammalian cells when stabilized and stored at non-cryogenic and cryogenic temperatures. In this interview, Chakraborty discusses the role that Raman spectroscopy plays in his work on biopreservation.

***Spectroscopy:* What are the advantages of Raman spectroscopy for your field of research?**

Chakraborty: I work in the field of biopreservation and my principal interest is the development of biopreservation techniques guided by physical characterization of intracellular environment.

During processing of cells for preservation, numerous biomolecules can be created within the cells that can ultimately be responsible for cell death or injury.

Raman spectroscopy allows us to chemically characterize cells with high resolution, thus providing an increased understanding of the possible nature of cellular injury in its native state. This technique can help us detect whether these molecules are getting created, where in the cells they are created, and how they are interacting with other molecules in the intracellular space.

It is possible to achieve a certain degree of this characterization with other techniques like fluorescence microscopy, but it's almost like a secondary mechanism. You cannot directly observe it. For example, with fluorescence microscopy, you need a fluorophore and other molecules to see what is going on. With Raman, the molecules themselves are enough to do that.

***Spectroscopy:* For which type of applications do you mainly use Raman imaging in your lab?**

Chakraborty: In our lab, we are focusing on special techniques related to low-temperature Raman imaging where the

intracellular environment is characterized at liquid nitrogen temperatures.

Currently, cells are preserved at very low cryogenic temperatures, at least below –80 degrees Celsius. While there are several theories at place, no one has direct proof of the actual mechanism that helps in stabilizing cells at low temperature. It is only after thawing that you can see whether the cell is alive or not.

Raman spectroscopy can help provide a fuller understanding of what is going on in the intracellular space that leads to successful storage at low temperatures. This technique enables us to look inside the cell in very low temperatures to understand why some cells are getting preserved and others are not.

Spectroscopy: **How has Raman instrumentation evolved over the past several years, what do you expect to come in the future?**

Chakraborty: For many years, Raman instrumentation was only used for characterization in non-biological materials. This instrumentation has been evolving in ways that expand its capabilities in several capacities. Some important aspects that enable the technique to be suitable for biological work are confocality, spatial resolution, spectral resolution, and reduction in excitation laser power requirement. I expect each of these aspects to continue evolving in favor of biological applications. I believe we will also see a significant increase in the development of reference biological databases in Raman spectroscopy.

The two things that have made the biggest impact on my work have been improvements in confocality (i.e., the ability to stay on a focal plane and collect information from that plane) and hyperspectral imaging (i.e., combining spectral and spatial information together create a chemical image).

Spectroscopy: **Combining different microscopy techniques for a more comprehensive understanding of the properties of a sample is an ongoing trend in the scientific community. Are there any approaches in your research group toward correlating Raman imaging with other techniques?**

Chakraborty: Our group is already working on combining low-temperature, light-sheet microscopy, and fluorescence microscopy aspects with Raman microspectroscopy.

While true spatial correlation is important when combining multiple microscopy or spectroscopy techniques, it is also important to make sure that the system remains friendly to live cell imaging techniques. In this regard, improved confocality of the system will play an important role. Current trends in in-vitro biological studies are moving toward physiologically relevant 3D cellular structures and the ability to collect 3D spectroscopical information using more than one microscopy or spectroscopy technique will be highly appealing. If we can successfully do that, I believe then only we will be realizing the full potential of Raman microspectroscopy. ■

CONFOCAL RAMAN MICROSCOPY IN FORENSIC PHARMACEUTICAL INVESTIGATIONS

Mary A. Miller, Michelle R. Cavaliere, Ming Zhou, and Pronda Few

Scanning electron microscopy with energy dispersive X-ray spectrometry (SEM-EDS) and Fourier-transform infrared microspectrophotometry (micro-FT-IR) have been widely demonstrated as complementary analytical tools for the identification of complex mixtures and unknown materials. However, there is a gap between the information provided by these two techniques. Even though elemental and morphological information is obtained on small single particles with SEM-EDS technology, no molecular or structural information is available. Likewise, although chemical information can be acquired using FT-IR, analysis of small single particles is significantly limited. We applied confocal Raman microscopy (CRM) in our laboratory to bridge the gap between FT-IR and SEM, and it provided chemical and vibrational information on a scale approaching the resolution of an SEM. In one application, monomer solutions used during a contact lens manufacturing process exhibited haze that was related to particulate contamination. The particles were isolated and analyzed by CRM, SEM, and micro-FT-IR. The particle size range was about 1–500 µm. Particles <50 µm were analyzed and

identified by Raman spectroscopy and SEM. Particles >50 µm were analyzed and identified by micro-FT-IR and SEM. Numerous materials associated with the manufacturing process of the monomer were identified, as well as foreign materials. The identification of the particulate materials causing the haze of the monomer assisted the manufacturer in determining the sources of the contamination and improving the quality of the product.

Raman spectroscopy is an ideal technique for analyzing product contaminants. Many materials can be identified by their Raman spectra, including minerals, dyes and pigments, polymers, and drugs. Raman microscopy has high spatial resolution, excellent sensitivity, and can quickly obtain spectral data. The technique often requires little-to-no sample preparation, and it is possible to collect spectra of materials through glass, plastics, and aqueous solutions. The ability to acquire spectral data without sample preparation limits accidental contamination and loss of the particle or material of interest (1). The technique is nondestructive in most applications. Confocal Raman microscopy (CRM) is especially useful for obtaining depth profiles (*x*–*z* scans) without conventional cross-sectioning of the samples (2–4). The ability to obtain vibrational spectra of small particles (<1–50 µm) complements the data obtained by the more traditional techniques of micro Fourier-transform infrared (micro-FT-IR) and scanning electron microscopy with energy dispersive X-ray spectrometry (SEM-EDS) (5–7). Raman spectroscopy is a particularly useful method for applications in the pharmaceutical, biomedical device, and consumer health products industries.

Janet Woodcock's article "The Concept of Pharmaceutical Quality" describes the Food and Drug Administration's (FDA) perspective on the quality of pharmaceuticals and highlights the efforts and financial resources invested to protect the health and safety of consumers (8). Forensic investigations in the pharmaceutical industry began with examinations of counterfeit and adulterated drug products (9,10). This area now extends to quality-related issues in manufacturing processes, including consumer health products, drug tablets and capsules, implantable medical devices, surgical equipment and supplies, and ophthalmic lenses.

Monomer solutions are used in a variety of applications, including hard and soft contact lenses; a novel application reported in the literature is the use of contact lenses for delivery of controlled release drugs directly to the eye (11). Contamination of the monomer may reduce biocompatibility and permeability of the lens. Not only is the biocompatibility of the polymer important, it also must be produced in such a way that any residual monomer or solution does not pose a health risk (12). In general,

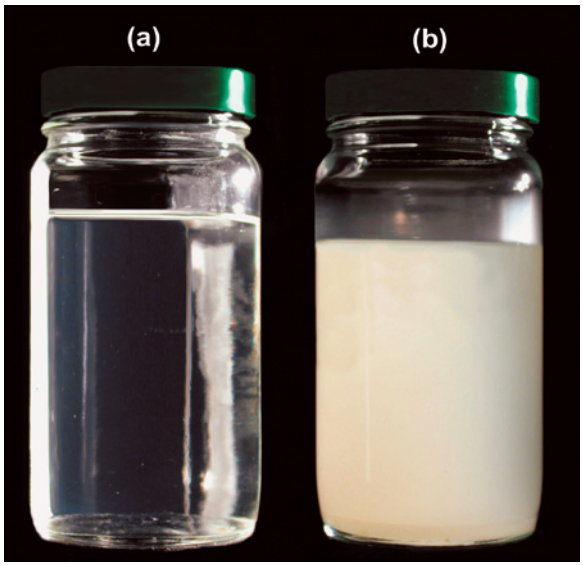

Figure 1: (a) Clear (least hazy) transparent monomer solution; (b) haziest monomer solution.

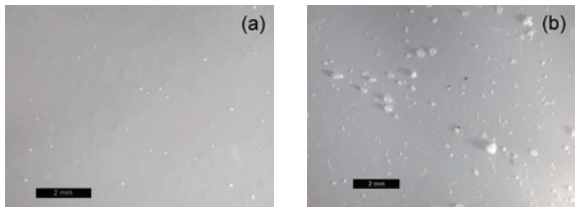

Figure 2: Photomicrographs showing isolated particulate materials on filter membranes from (a) least hazy solution and (b) haziest solution.

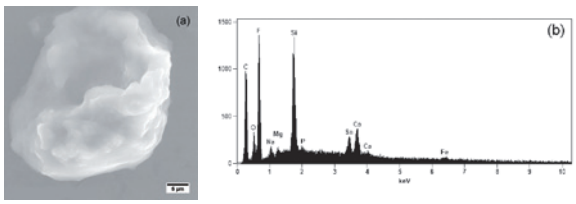

Figure 3: (a) SEM image of bumpy, textured particle isolated from least hazy monomer solution; (b) EDS spectrum from particle shown in (a).

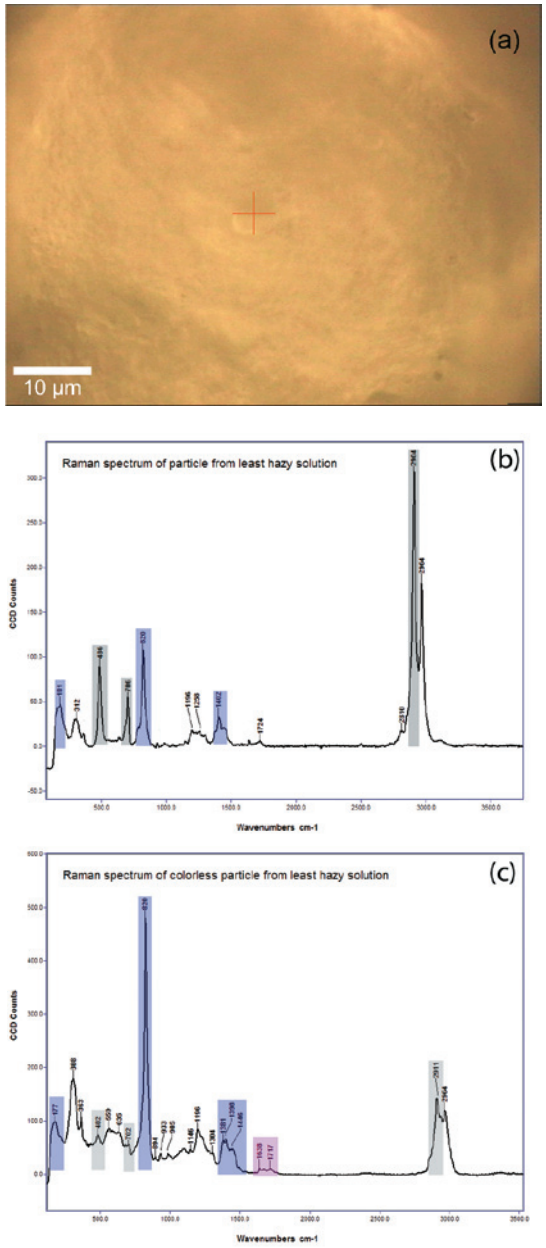

Figure 4: (a) Representative image of bumpy, textured particle selected for Raman analysis; (b) Raman spectrum of particle in (a), primarily fluoropolymer (blue) and monomer (grey); (c) Raman spectrum from additional clear or colorless particle showing a mixture of fluoropolymer (blue) and monomer (grey) with traces of isocyanate (pink). Refer to Table I for peak color codes of monomer and raw materials.

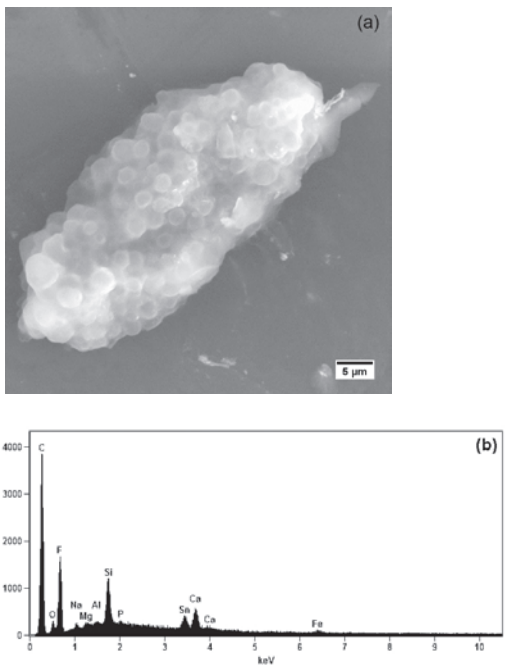

Figure 5: (a) SEM image of clear or colorless particle from the haziest monomer solution exhibiting bead-like features in a gel matrix; (b) EDS spectrum from particle indicates it is carbon (C), oxygen (O), fluorine (F), and silicon (Si) rich.

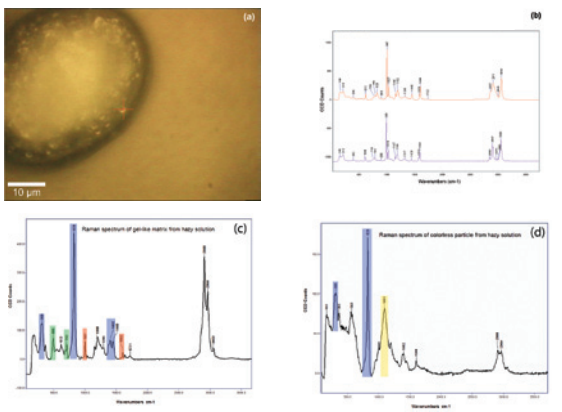

Figure 6: (a) Confocal Raman microscope image showing bead-like features observed in particles isolated from the haziest monomer solution; (b) Raman spectrum obtained from bead-like feature (upper trace) and a polystyrene reference spectrum (lower trace); (c) Raman spectrum of gel-like matrix consistent with fluoropolymer (blue), with traces of polystyrene-like compound (orange), and silicone (green); (d) Raman spectrum of clear or colorless particle consistent with mixture of fluoropolymer (blue) and isocyanate (yellow). Refer to Table I for color codes of monomer and raw materials.

high quality, inclusion-free polymers are equally important to all industries where a transparent polymer is required. Depending on the application, inclusions may result in reduced visibility and unintentional reflection or refraction of light.

In a recent case, inspection of monomers intended for use in the production of lenses revealed hazy solutions. These monomers did not meet the standard criteria for the final product manufacture, which requires a colorless, transparent polymer lens. MVA Scientific Consultants (Duluth, Georgia) was asked to investigate the nature of the haze in the monomer and intermediate product solutions and determine the source of the problem. The monomer is a proprietary formula consisting of multiple components, including but not limited to, silicone, fluoropolymer, organotin, acrylic, and isocyanate compounds.

This article describes the use of confocal Raman microscopy for the identification of particles in the 5–50 µm range and illustrates how it bridges the gap between micro-FT-IR and SEM-EDS analyses. The use of these complementary techniques in the pharmaceutical and allied industries is widely reported in the literature, especially for analyses and identification of small particles (6,7,10,13–16).

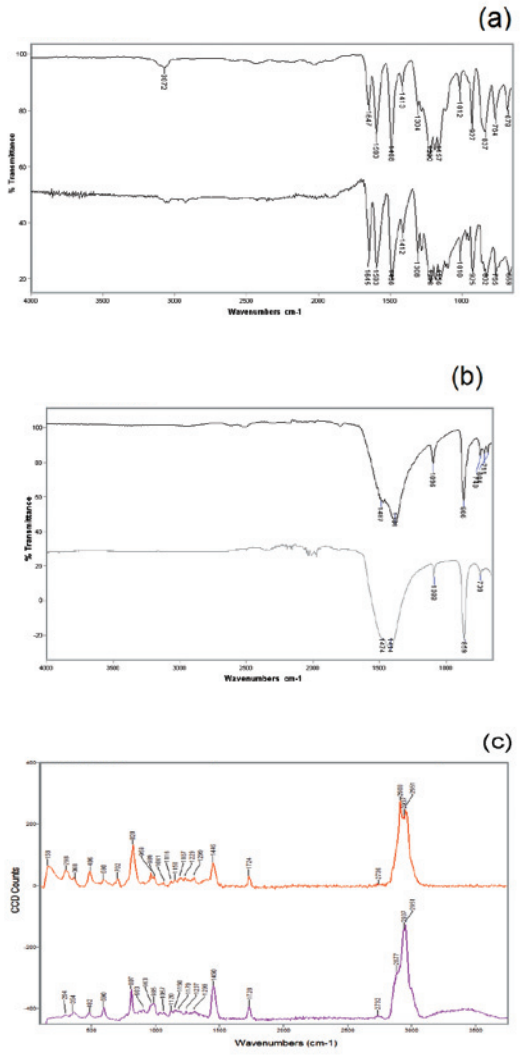

Figure 7: (a) Infrared spectrum (upper trace) of particle identified as extraneous material isolated from haziest monomer solution and polyether ether ketone (PEEK) reference (lower trace); (b) infrared spectrum (upper trace) of particle identified as extraneous material isolated from haziest monomer solution and inorganic carbonate reference (lower trace); (c) Raman spectrum (upper trace) of opaque or white particle identified as extraneous material isolated from haziest monomer solution and Carboset acrylic reference (lower trace).

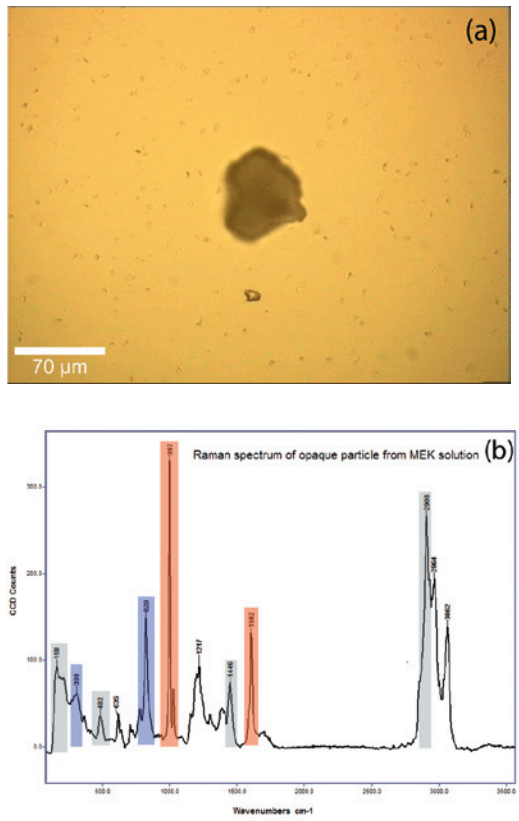

Figure 8: (a) Confocal Raman microscope image of opaque or white particle from MEK-diluted intermediate solution selected for Raman analysis; (b) Raman spectrum of particle in (a) suggests a mixture of fluoropolymer (blue), residual intermediate product or monomer (grey), and polystyrene (orange). Refer to Table I for color codes of monomer and raw materials.

Experimental

Preliminary examination of the monomer solutions and particulate material was conducted using a Zeiss Stemi-C2000 stereomicroscope (Carl Zeiss Microscopy, Thornwood, New York) with a magnification range of 6.5–47×. The monomer solutions were filtered in an ISO Class 5 clean bench for isolation of particulate material using GE Water and Process Technologies (Trevose, Pennsylvania) 47-mm diameter, 0.8-µm pore size, polycarbonate track etch membrane filters. The filters were rinsed

Table I: Raman peak frequencies (cm^{-1}) of monomer and raw materials

Isocyanate Compound 1	Isocyanate Compound 2	Silicone	Organotin	Fluoropolymer	Methyl Ethyl Ketone	Intermediate Product	Monomer
1091 (br)	3108	2904	1299	820	2921	3121	3108
559	2742	486	2854	300	755	2964	2964
2418	2425	702	1438	1454	1082	2904	2904
781	1717	186	1154	1380-1410	581	2810	2807
2538 (sh)	1638	1258	2911	177	1709	2415	2496
						1724 (w)	1721
						1450	1638
						1410	1446
						1299	1406
						1258	1295
						1082 (br)	1258
						781	855
						702	781
						482	702
						177	482
							186
							158

Key peak positions used for identification/correlation of components within mixtures
sh = shoulder, br = broad, w = weak

with prefiltered (0.2 µm) ethanol. Ethanol blanks and controls were prepared and examined with each sample set to ensure no introduction of significant particulate material during sample preparation. Representative particles were selected using fine tungsten microtools for analyses by micro-FT-IR, SEM-EDS, and CRM.

Micro-FT-IR analyses were conducted with a SensIR IlluminatIR Fourier transform infrared spectrophotometer (Smiths Detection, Danbury Connecticut, formerly SensIR Technologies, Danbury, Connecticut) coupled to an Olympus BX-51 compound microscope (Olympus America, Center Valley, Pennsylvania). Spectra were collected using a 50- or 100-µm aperture, a spectral resolution of 4 cm^{-1}, 128 scans, and either an all reflecting objective (ARO) or an attenuated total internal reflectance (ATR) objective.

JEOL JSM-6400 and JSM-6500F scanning electron microscopes (JEOL USA, Inc., Peabody, Massachusetts) with Noran energy dispersive X-ray systems (Thermo Scientific Noran, Madison, Wisconsin) were used for SEM-EDS analyses.

Raman spectra were obtained using a WITec (Maryville, Tennessee) alpha 300R confocal Raman microscope with a 532-nm excitation wavelength laser (NdYAG). Images of the particles were obtained before analyses. Typical spectra were collected using a 20× Nikon or a 100×

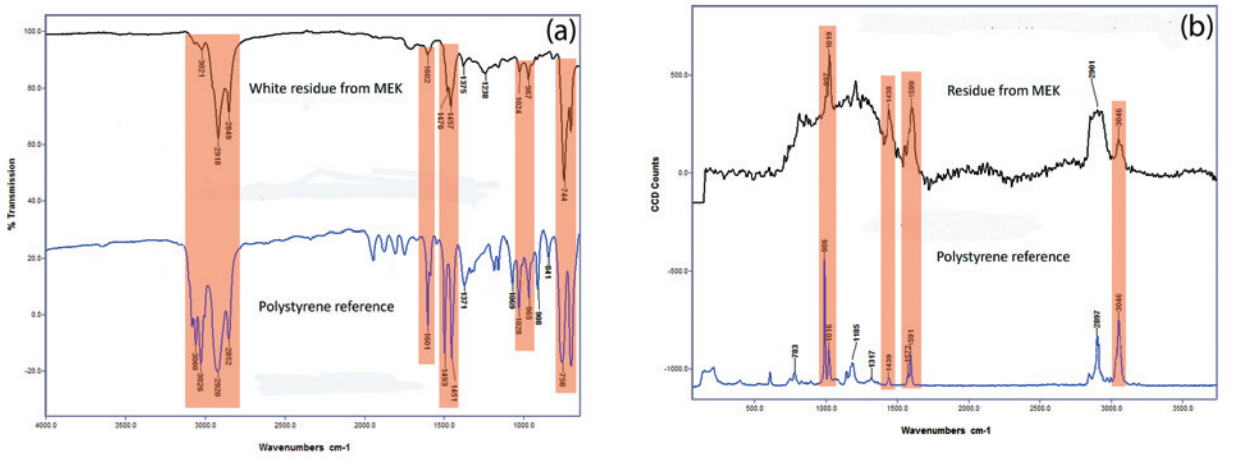

Figure 9: Infrared and Raman spectra of white residue recovered from MEK solvent: (a) Infrared spectra of residue (upper trace) and polystyrene reference (lower trace); (b) Raman spectra of residue (upper trace) and polystyrene reference (lower trace). Highlighted peaks illustrate correlation.

Olympus objective, a 0.1-s integration time, and 100 accumulated scans. The spectrometer grating used was 600 grooves/mm. Both Raman and FT-IR spectra were processed using Thermo Electron Grams AI software (Thermo Fisher Scientific, Madison, Wisconsin).

Results and Discussion

Visual Inspection

More than 20 samples of the monomer solutions were received. The solutions were visually inspected and ranked based on the level of visual clarity and haziness. Preliminary examination suggested the haze was caused by particles in the solutions. Representative samples of the least and most hazy solutions were selected for analyses. Figure 1 shows the representative samples.

The two solutions were filtered and particles were retained on the filter membranes, as shown in Figure 2. The predominant particles recovered from the hazy solution had a size range of approximately 20–500 µm. Stereoscopic examination of the filters revealed fine, white-to-colorless particles; opaque-to-transparent flakes and ribbons; brown, red, and orange-yellow particles; colorless, red, tan, and blue fibers; and large fibrous masses.

Examination of Particulate Isolated from the Least Hazy Solution

Particles from the least hazy monomer solution ranged in size from about 25 to 150 µm and were primarily clear or colorless and opaque or white. The approximate total weight percent of particulate (post-sampling) isolated from this sample was 0.001%. SEM analysis revealed that most of the particles had a bumpy, textured surface (Figure 3a). The

elemental composition of a typical particle (Figure 3b) is consistent with components of the monomer solution including the fluoropolymer and silicone compounds with traces of the organotin compound and other inorganic salts. Analysis by Raman microscopy confirmed highly textured surfaces; a representative image is presented in Figure 4a. The Raman spectra suggested the particles were composed of silicone compounds and fluoropolymer with traces of an isocyanate compound (Figures 4b and 4c) — all components of the monomer solution.

Examination of Particulate Isolated from the Haziest Solution

Several clear or colorless and opaque or white particles in the 20–200 µm range were isolated from the haziest solution for evaluation. The approximate total weight percent of particulate (post-sampling) isolated from this sample was 0.004%. Examination of the 20–200 µm isolated particles by SEM revealed that most were composed of small bead-like features held together by a gelatinous material (Figure 5a). EDS analysis of these particles yielded elemental compositions rich in carbon, oxygen, silicon, and fluorine, with traces of calcium, sodium, and tin present (Figure 5b). Confocal Raman microscopy was used to characterize the small bead-like particles within the gelatinous matrix, many of which were <5 µm in diameter. This technique was especially effective because it allowed us to focus directly on the beads without further isolation from the gelatinous material. A representative particle exhibiting bead-like features is shown in the micrograph presented in Figure 6a; the corresponding Raman spectrum acquired from the marked location is shown in Figure 6b. Matching this Raman spectrum to spectral databases revealed the beads were consistent with a polystyrene-like material (Figure 6b). Raman spectral analysis of the gel-like matrix and colorless irregular shaped particles revealed mixtures of the components in the monomer solution, primarily fluoropolymer, silicone, and isocyanate (Figures 6c and 6d). The peaks at 997 cm^{-1} and 1602 cm^{-1} in Figure 6c suggest a trace of a polystyrene-like compound also may be present.

Extraneous materials were identified by micro-FT-IR and Raman spectroscopy. The FT-IR spectrum of a 70-µm clear particle indicated that the particle was a polyether ether ketone (PEEK) polymer (Figure 7a). Another clear particle was characterized as an inorganic carbonate by FT-IR spectroscopy and is presented in Figure 7b. Analysis of white particles by Raman spectroscopy with spectral matching revealed an acrylic polymer consistent with Carboset (Lubrizol Advanced Materials, Inc., Wickliffe, Ohio) products. Representative Raman spectra are presented in Figure 7c. Other extraneous materials identified by light microscopy, FT-IR, and Raman spectroscopy included skin flakes, cellulose particles and fibers (paper, cotton), polyethylene, and poly(tetrafluoroethylene) or PTFE.

Examination of Raw Materials, Intermediate Product, and Process Solvent

To trace the origin of the particles causing the haziness of the monomer solutions, the raw materials and processing solvent were evaluated. A sample of an intermediate product of the polymer (that is, a prepolymerized, viscous liquid that had not yet been cross-linked) also was provided. Evaluation of the Raman and FT-IR spectra obtained from the starting materials, the methyl ethyl ketone processing solvent, the monomer solution, and the prepolymerized intermediate product revealed spectral peaks that could be used as markers for identification of these compounds in particles isolated from the monomer solutions. The spectra obtained from the intermediate product and the monomer solutions were quite similar and distinctions between the two were based on subtle variations of the contributions of the two isocyanate compounds. When identifying particles, the distinction between the monomer and intermediate product is not made, so both are referred to as monomer. The key peak positions for the raw materials, methyl ethyl ketone solvent, intermediate product, and monomer are provided in Table I.

Dilution of the viscous intermediate product solution with methyl ethyl ketone, followed by filtration, yielded clear or colorless and opaque or white particles that ranged in size from approximately 20 to 400 µm. Representative particles were selected for analysis by FT-IR, Raman microscopy, and SEM-EDS. FT-IR analyses of selected particles revealed materials associated with the monomer components, primarily fluoropolymer and silicone. Both surface texture and the elemental composition were evaluated by SEM-EDS. The data indicate bumpy, textured particle morphologies mainly composed of carbon, oxygen, silicon, and fluorine. Raman analyses showed that most of the particles were mixtures of the monomer components, primarily the fluoropolymer and isocyanate. (These data are consistent to the spectra presented in Figures 4, 6c, and 6d.)

Extraneous materials recovered from the viscous intermediate product following dilution with methyl ethyl ketone were identified by SEM-EDS and Raman microscopy. A representative 300-µm opaque or white particle was selected for analysis by SEM-EDS; the elemental composition is consistent with silicon. One 70–80 µm clear or colorless particle yielded a Raman spectrum consistent with an acrylic material, such as the Carboset acrylic material previously observed. An opaque or white particle exhibiting a bumpy, textured surface is shown in Figure 8a. The Raman spectrum of this particle indicates it is a mixture of fluoropolymer, residual monomer or intermediate product, and a polystyrene-like compound (Figure 8b).

The results of the preparation of the intermediate with methyl ethyl ketone led

to the investigation of the methyl ethyl ketone solvent as a potential source of the polystyrene-like material. Evaporation of the methyl ethyl ketone yielded insufficient residue for analyses. A small volume (2 mL) of remaining methyl ethyl ketone solvent was mixed with particle-free deionized water to reduce the solubility of any polystyrene, if present, in the solvent. During the addition of the water to the methyl ethyl ketone, a small amount of white residue was observed forming on the container walls, immediately above the liquid level. Evaporation of the methyl ethyl ketone and water blend yielded additional white residue for evaluation. However, the overall residue collected was minimal; the amount was estimated to be in the microgram range based on the overall weight percents of particulate collected from the monomer solutions and volume of methyl ethyl ketone used for the dissolution and evaporation study. FT-IR and Raman spectroscopy were used for analyses of the white residue and yielded spectra that suggested polystyrene or a related aromatic impurity was present in the methyl ethyl ketone solvent. The FT-IR spectra are presented in Figure 9a, and the corresponding Raman spectra are shown in Figure 9b.

Conclusion

Analyses of monomer and intermediate product solutions exhibiting particulate materials led to the evaluation of the raw materials and processing solvents as potential sources of extraneous particles. Most of the particles in the least hazy solution were determined to be related to the starting materials used in the formulation. Results indicated that most of the particles were mixtures of monomer components. Extraneous materials not related to components of the monomer were also identified.

Differences between the least hazy and haziest monomer solutions were primarily due to the presence of 2–10 µm polystyrene beads encapsulated in gel-like aggregated clumps of mixtures of the monomer components in the haziest solution. These individual polystyrene beads were identified using the high spatial resolution capabilities provided by CRM. The polystyrene-like component was rare or absent in the least hazy solution. The polystyrene contamination was traced back to the methyl ethyl ketone solvent. Although FT-IR spectroscopy suggested polystyrene might be present, Raman microscopy provided supporting results indicating the presence of a polystyrene-like material; detection of small particles of extraneous polystyrene-like material demonstrates the advantages achieved with confocal Raman microscopy.

The use of FT-IR and Raman spectroscopy along with SEM-EDS provided complementary analytical results to solve a challenging quality control problem during a contact lens manufacturing process. Identification of the particulate materials causing the haze of the monomer, as well as the source of it, assisted the manufacturer in improving the quality of the product.

References

(1) E. Caudron, A. Tfayli, C. Monnier, M. Manfait, P. Prognon, and D. Pradeu, *J. Pharm. Biomed. Anal.* **54,** 866–868 (2011).

(2) T. Vankeirsbilck, A. Vercauteren, W. Baeyens, and G. Van der Weken, *Trends Anal. Chem.* **21,** 869–877 (2002).

(3) M. Miller, M. Cavaliere, and D. Drew, "Evaluation of Controlled Release Products by Light Microscopy, Scanning Electron Microscopy and Confocal Raman Microscopy," presented at 37th Annual Meeting and Exposition of the Controlled Release Society, Portland, Oregon, 2010.

(4) M. Cavaliere, M. Miller, and T. Vander Wood, "Microscopical Characterization of Controlled Release Pharmaceuticals: A Complementary Approach," proceedings of Microscopy and Microanalysis, Portland, Oregon, 2010. J. Shields, S. McKernan, J. Mansfield, B. Foran, J. Frafjord, D. Beniac, and D. O'Neil, Eds. (Cambridge University Press, New York, New York, 2010).

(5) M. Miller, "Identification of Impurities in a Pharmaceutical API: Is Meeting USP Compendial Testing Enough?," presented at the American Association of Pharmaceutical Scientists (AAPS) Annual Meeting and Exposition, Los Angeles, California, 2009.

(6) M.A. Miller and T.B. Vander Wood, "Microanalysis in the Pharmaceutical and Biomedical Industry," proceedings of Microscopy and Microanalysis, San Antonio, Texas, 2003; D. Piston, J. Bruley, I.M. Anderson, P.Kotula, G. Solorzano, A. Lockley, and S. McKernan, Eds. (Cambridge University Press, New York, New York, 2003).

(7) T. Barber, *Instrumental Analysis of Particulate Matter, in Liquid-and Surface-Borne Particle Measurement Handbook*, J. Knapp, T. Barber, and A. Lieberman, Eds. (Marcel Dekker, New York, New York, 1996).

(8) J. Woodcock, *Amer. Pharma. Rev.* **7,** 10–15 (2004).

(9) N. Macleod and P. Matousek, *Pharm. Res.* **25,** 2205–2215 (2008).

(10) M. Witkowski, *Amer. Pharma. Rev.* **8,** 1–5 (2005).

(11) C. Alvareze-Lorenzo, H. Haruyuki, and A. Concheiro, *Amer. J. Drug Deliv.* **4,** 131–151 (2006).

(12) J. Bergin, "Contact Lens Polymers: A Technical Overview of the Development, Manufacturing, and Future of Contact Lenses," presentation from Introduction to Polymers Course, State University of New York at Buffalo, Buffalo, New York, 2000.

(13) D. Alonso, "Microscopy Techniques in Pharmaceutical and other Manufacturing Industries," proceedings of Microscopy and Microanalysis, Honolulu, Hawaii, 2005. R. Price et al., Eds. (Cambridge University Press, New York, New York, 2005).

(14) D.S. Aldrich, "Particulate Matter in Air and in Liquids- Isolation, Quantitation and Identification Considerations," proceedings of Microscopy and Microanalysis, Honolulu, Hawaii, 2005. R. Price et al., Eds. (Cambridge University Press, new York, New York, 2005).

(15) G. Torraca and Z. Wen, "Forensic Investigation of Biopharmaceutical Manufacturing Incidents by Light Microscopy, FT-IR Microscopy, Scanning Electron Microscopy and Energy Dispersive X-ray Spectrometry," proceedings of Microscopy and Microanalysis, Honolulu, Hawaii, 2005. R. Price et al., Eds. (Cambridge University Press, New York, New York, 2005).

(16) F. Adar, G. leBourdon, J. Reffner, and A. Whitley, *Spectros.* **18**(2), 34–40 (2003).

At the time of publication, **Mary A. Miller, Michelle R. Cavaliere, Ming Zhou,** *and* **Pronda Few** *were with MVA Scientific Consultants in Duluth, Georgia. Direct correspondence to: mmiller@mvainc.com.*

This piece originally appeared in *Spectroscopy* **27** (2), 48–59 (2012). ■